

**Effect of Cold Temperature on the Dielectric
Constant of Soil**

**by Gregory J. Mazzaro, Gregory D. Smith, Getachew Kirose,
and Kelly D. Sherbondy**

ARL-TN-0479

April 2012

NOTICES

Disclaimers

The findings in this report are not to be construed as an official Department of the Army position unless so designated by other authorized documents.

Citation of manufacturer's or trade names does not constitute an official endorsement or approval of the use thereof.

Destroy this report when it is no longer needed. Do not return it to the originator.

Army Research Laboratory

Adelphi, MD 20783-1197

ARL-TN-0479

April 2012

Effect of Cold Temperature on the Dielectric Constant of Soil

**Gregory J. Mazzaro, Gregory D. Smith, Getachew Kirose,
and Kelly D. Sherbondy**
Sensors and Electron Devices Directorate, ARL

REPORT DOCUMENTATION PAGE

Form Approved
OMB No. 0704-0188

Public reporting burden for this collection of information is estimated to average 1 hour per response, including the time for reviewing instructions, searching existing data sources, gathering and maintaining the data needed, and completing and reviewing the collection information. Send comments regarding this burden estimate or any other aspect of this collection of information, including suggestions for reducing the burden, to Department of Defense, Washington Headquarters Services, Directorate for Information Operations and Reports (0704-0188), 1215 Jefferson Davis Highway, Suite 1204, Arlington, VA 22202-4302. Respondents should be aware that notwithstanding any other provision of law, no person shall be subject to any penalty for failing to comply with a collection of information if it does not display a currently valid OMB control number.

PLEASE DO NOT RETURN YOUR FORM TO THE ABOVE ADDRESS.

1. REPORT DATE (DD-MM-YYYY) April 2012	2. REPORT TYPE	3. DATES COVERED (From - To) December 2011 to January 2012			
4. TITLE AND SUBTITLE Effect of Cold Temperature on the Dielectric Constant of Soil		5a. CONTRACT NUMBER			
		5b. GRANT NUMBER			
		5c. PROGRAM ELEMENT NUMBER			
6. AUTHOR(S) Gregory J. Mazzaro, Gregory D. Smith, Getachew Kirose, and Kelly D. Sherbondy		5d. PROJECT NUMBER			
		5e. TASK NUMBER			
		5f. WORK UNIT NUMBER			
7. PERFORMING ORGANIZATION NAME(S) AND ADDRESS(ES) U.S. Army Research Laboratory ATTN: RDRL-SER-U 2800 Powder Mill Road Adelphi, MD 20783-1197		8. PERFORMING ORGANIZATION REPORT NUMBER ARL-TN-0479			
9. SPONSORING/MONITORING AGENCY NAME(S) AND ADDRESS(ES)		10. SPONSOR/MONITOR'S ACRONYM(S)			
		11. SPONSOR/MONITOR'S REPORT NUMBER(S)			
12. DISTRIBUTION/AVAILABILITY STATEMENT Approved for public release; distribution unlimited.					
13. SUPPLEMENTARY NOTES					
14. ABSTRACT The effect of cold temperature on the dielectric constant of moist soil is studied. Three soil samples are measured at three moisture levels, at temperatures between -30 and +30 °C, and at seven frequencies relevant to ground-penetrating radar. It is found that for dry soil, cold temperatures have little effect on the dielectric constant. Further, for soils with medium-to-high moisture content, there is a downward trend in both the real and the imaginary parts of the dielectric constant with colder temperatures. For dry soils, the performance of radar sensors is expected to remain steady at cold temperatures. For medium and high moisture content soils, an increase in soil-to-target contrast as well as radar penetration into the soil is expected.					
15. SUBJECT TERMS Dielectric, temperature, measurement, cold, ring resonator, soil, moisture, ground-penetrating radar					
16. SECURITY CLASSIFICATION OF:			17. LIMITATION OF ABSTRACT UU	18. NUMBER OF PAGES 28	19a. NAME OF RESPONSIBLE PERSON Gregory J. Mazzaro
a. REPORT Unclassified	b. ABSTRACT Unclassified	c. THIS PAGE Unclassified			19b. TELEPHONE NUMBER (Include area code) (301) 394-0840

Contents

List of Figures	iv
Acknowledgment	v
1. Introduction	1
2. Dielectric Constant and the Ring-resonator Concept	1
3. Measurement Equipment	5
4. Measurement Procedure	7
5. Dielectric Constant Data	10
6. Conclusion	17
7. References	18
Appendix. Effect of Cold Temperature on the Ring-Resonator Measurement System	19
Distribution List	20

List of Figures

Figure 1. Traditional ring-resonator structure. For the 1200-MHz resonator used in this study, $h = 508 \mu\text{m}$, $r_i = 23.0 \text{ mm}$, $r_o = 24.1 \text{ mm}$, $w = 1.11 \text{ mm}$, $c_i = 24.7 \text{ mm}$, $c_o = 25.8 \text{ mm}$, $d = 17.0 \text{ mm}$, $s_i = 37.0 \text{ mm}$, and $s_o = 37.5 \text{ mm}$.	3
Figure 2. Compact ring resonator and sample placement required for ϵ_r measurement: (a) resonator left unloaded, and (b) resonator loaded by dielectric sample.	4
Figure 3. Data traces for permittivity measurement, before and after dielectric loading.	4
Figure 4. Thermotron S-C8 temperature-controlled chamber: (a) outside and (b) inside.	6
Figure 5. Measurement apparatus: (a) ring-resonator system and (b) temperature monitor.	7
Figure 6. Measurement procedure flowchart.	8
Figure 7. Data capture example: (a) place the ring resonator in flush contact with the sample and (b) record the associated $ S_{21} $ trace on the VNA.	8
Figure 8. N9923A_ringres GUI: the sample-absent trace is shown in blue; the sample-present trace is shown in red.	9
Figure 9. Dielectric constant (real part) vs. temperature and moisture, APG soil.	10
Figure 10. Dielectric constant (real part) vs. temperature and moisture, Ft. Irwin soil.	11
Figure 11. Dielectric constant (real part) vs. temperature and moisture, YPG soil.	11
Figure 12. Dielectric constant (imaginary part) vs. temperature and moisture, APG soil.	12
Figure 13. Dielectric constant (imaginary part) vs. temperature and moisture, Ft. Irwin soil.	12
Figure 14. Dielectric constant (imaginary part) vs. temperature and moisture, YPG soil.	13
Figure 15. Dielectric constant (real part) vs. temperature, APG soil.	13
Figure 16. Dielectric constant (real part) vs. temperature, Ft. Irwin soil.	14
Figure 17. Dielectric constant (real part) vs. temperature, YPG soil.	14
Figure 18. Dielectric constant (imaginary part) vs. temperature, APG soil.	14
Figure 19. Dielectric constant (imaginary part) vs. temperature, Ft. Irwin soil.	15
Figure 20. Dielectric constant (imaginary part) vs. temperature, YPG soil.	15
Figure A-1. Dielectric constant (imaginary part) vs. temperature, YPG soil.	19

Acknowledgment

We would like to thank the following people for their assistance during this study: Abraham (Ami) Frydman for granting access to the Thermotron cold chamber and Rene Ramirez for preparing the chamber for measurements and providing instructions on its proper use.

INTENTIONALLY LEFT BLANK.

1. Introduction

A sensing modality under investigation by the U.S. Army for detecting improvised explosive device (IED) threats is ground-penetrating radar (GPR). Proper development of GPR technology for this application requires a unique understanding of the electromagnetic (EM) properties of targets and their surrounding media. Thus, the EM characterization of soils is fundamental to the success or failure of GPR as a detection technique.

One soil property of interest to radar engineers is the dielectric constant. Previous investigations by the U.S. Army Research Laboratory (ARL) have found that the dielectric constant of soil can vary widely depending on its type, terrain, and moisture content (1). Recently, ARL was asked by the Joint Improvised Explosive Device Defeat Organization (JIEDDO) Joint Test Board (JTB) to investigate the variation of the soil dielectric constant with temperature.

Using a recently developed in-situ dielectric measurement system developed by the Sensors and Electron Devices Directorate (2), as well as an in-house temperature-controlled chamber, members of the Radio Frequency (RF) Signal Processing and Modeling Branch determined the dielectric constants of three soil samples, containing three different levels of moisture, at seven different frequencies, and at seven temperatures between -30 and $+30$ °C.

Prior research indicates a fairly linear rise with temperature in both components of the dielectric constant for soil containing low levels of moisture and a more step-like rise with temperature at greater levels of moisture (3–5). The step-change occurs near 0 °C and is apparently due to the phase change of the moisture from liquid to solid. This study aims to extend these results to temperatures, moisture levels, and frequencies relevant to GPR systems.

2. Dielectric Constant and the Ring-resonator Concept

The two constitutive parameters that govern the behavior of EM waves propagating in a radar environment are electrical permittivity ϵ and magnetic permeability μ . Since most materials encountered in operational scenarios are either non-magnetic or very weakly magnetic, it is primarily variations in permittivity along the path of a radar wave that dictate how the wave interacts with the environment.

For convenience, permittivity is usually normalized to that of free space (ϵ_0):

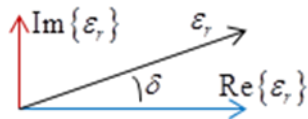
$$\epsilon_r = \frac{\epsilon}{\epsilon_0} = \epsilon_r' - j\epsilon_r'' = \text{Re}\{\epsilon_r\} + j \cdot \text{Im}\{\epsilon_r\}. \quad (1)$$

Values for ϵ_r are typically reported as positive although the imaginary part of ϵ_r is negative (for passive materials). Another name for the permittivity of a material relative to that of free space is “dielectric constant,” ϵ_r .

The “real” part of the dielectric constant $Re\{\epsilon_r\}$ is a measure of the EM contrast of between materials (e.g., between soil and a buried target). The greater the difference between two values of $Re\{\epsilon_r\}$, the greater the magnitude of the radar wave reflected from the interface between the two materials. A radar can more easily detect a target if the value of $Re\{\epsilon_r\}$ for that target differs greatly from its surrounding media.

The “imaginary” part of the dielectric constant $Im\{\epsilon_r\}$ is a measure of the attenuation experienced by an EM wave propagating through a material. The greater the value of $Im\{\epsilon_r\}$ for a material, the more quickly an EM wave attenuates with distance into the material. A radar can more easily penetrate into a material (e.g., down into a soil) when $Im\{\epsilon_r\}$ for that material is low.

In the relevant literature, “dielectric constant” often refers to the magnitude of ϵ_r . Also, attenuation is often represented in terms of the loss tangent, $\tan\delta$. The relationships between each of these quantities are those of a vector of magnitude $|\epsilon_r|$ and angle δ :



$$|\epsilon_r| = \sqrt{(\text{Re}\{\epsilon_r\})^2 + (\text{Im}\{\epsilon_r\})^2} \quad \tan\delta = \frac{\text{Im}\{\epsilon_r\}}{\text{Re}\{\epsilon_r\}}. \quad (2)$$

For most radar materials-of-interest including dry soils and slightly moist soils, $Im\{\epsilon_r\} \ll Re\{\epsilon_r\}$, such that $|\epsilon_r| \approx Re\{\epsilon_r\}$ and $\tan\delta \approx \delta$.

The apparatus employed to measure dielectric constant for this study is the ring resonator, depicted in figure 1. A ring resonator is a two-port transmission-line structure consisting of an input feedline, a closed-loop ring, an output feedline, and two coupling gaps (θ).

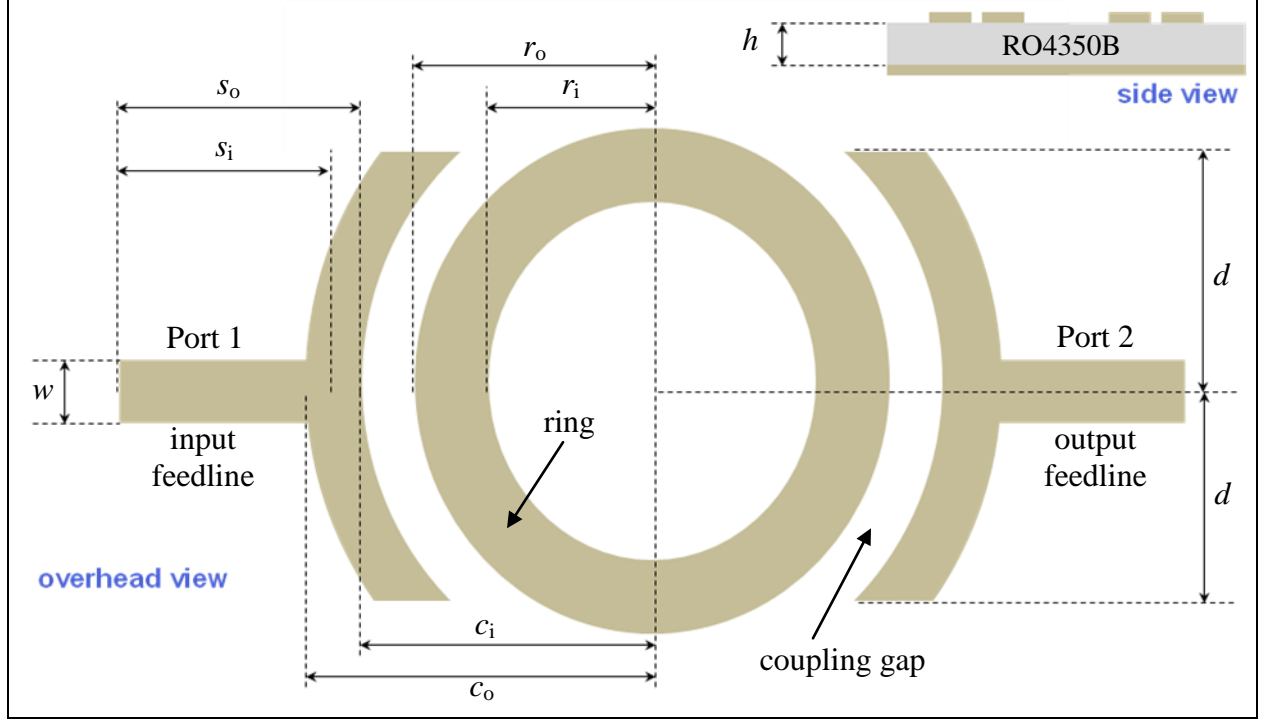


Figure 1. Traditional ring-resonator structure. For the 1200-MHz resonator used in this study, $h = 508 \mu\text{m}$, $r_i = 23.0 \text{ mm}$, $r_o = 24.1 \text{ mm}$, $w = 1.11 \text{ mm}$, $c_i = 24.7 \text{ mm}$, $c_o = 25.8 \text{ mm}$, $d = 17.0 \text{ mm}$, $s_i = 37.0 \text{ mm}$, and $s_o = 37.5 \text{ mm}$.

The ring and its feedlines are signal-carrying conductors in microstrip. Beneath the ring is a printed circuit board (PCB) of uniform thickness and dielectric constant, and beneath the PCB dielectric is a metal ground plane. RF energy couples into and out of the resonator via the feedlines and coupling gaps. Resonance is established when the circumference of the resonator is an integral multiple of the wavelength of RF propagating in the transmission line,

$$2\pi r = n\lambda_g \quad (3)$$

where r is the average radius of the ring, λ_g is the guided wavelength, and n is the mode number. The fundamental resonant frequency of the ring f_0 , corresponding to $n = 1$, is equal to

$$f_0 = \frac{v}{\lambda_g} = \frac{c}{\lambda_g \sqrt{|\epsilon_{\text{eff}}|}} = \frac{c}{2\pi r \sqrt{|\epsilon_{\text{eff}}|}} \quad (4)$$

where c is the speed of light in air and ϵ_{eff} is the effective dielectric constant of the unloaded transmission-line structure. At this frequency, the two-port transmission coefficient $|S_{21}|$, measured at the output feedline (Port 2) with respect to the input feedline (Port 1), reaches a local maximum. Maxima are also observed at $n = 2, 3, 4, \dots$, corresponding to $2f_0, 3f_0, 4f_0$, etc.

The change in the resonance of the ring measured in the presence of a sample (loaded) and that measured in the absence of the sample (unloaded) enables the calculation of the sample's

dielectric constant (ϵ_r). Figures 2 and 3 illustrate the measurement concept. First, the resonator is left unloaded, with only air occupying the space above the ring, as in figure 2a. Shown here is a compact resonator formed by using a meander-line structure in place of the traditional circular ring (2, 7). The transmission coefficient of the resonator in air is recorded using a network analyzer, as in figure 3. From this trace, the frequency at the resonant peak, f_u , and the quality factor of the resonance, Q_u , are noted. Next, the dielectric sample is placed on top of the resonator (or vice versa), as in figure 2b. The ring and the sample are pressed together so that the two are flush. A second data trace is recorded for the resonator loaded by the dielectric sample, as in figure 3. The new resonant frequency, f_l , and quality factor, Q_l , are noted. The shift in the peak of the resonance with respect to frequency indicates the “real” part of the dielectric constant, $Re\{\epsilon_r\}$. The widening of the peak of the resonance indicates the “imaginary” part of the dielectric constant, $Im\{\epsilon_r\}$.

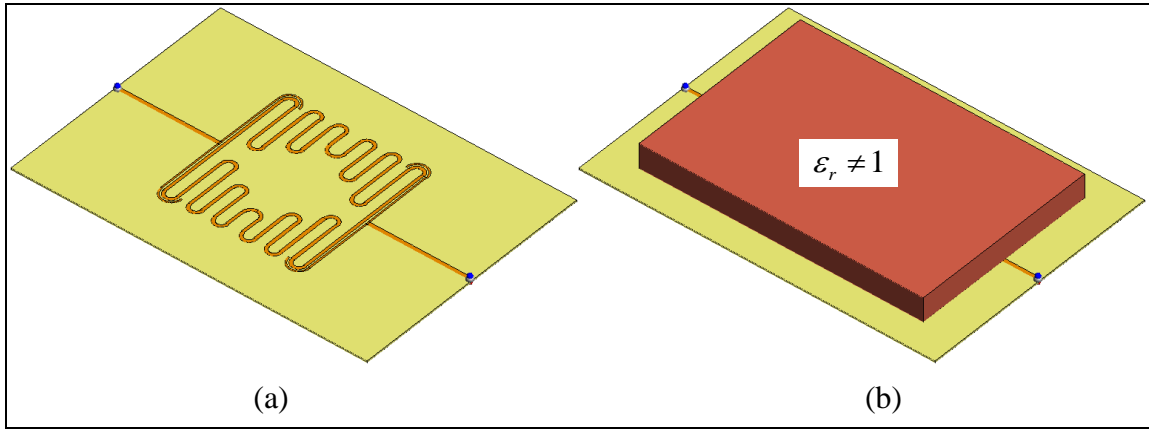


Figure 2. Compact ring resonator and sample placement required for ϵ_r measurement: (a) resonator left unloaded, and (b) resonator loaded by dielectric sample.

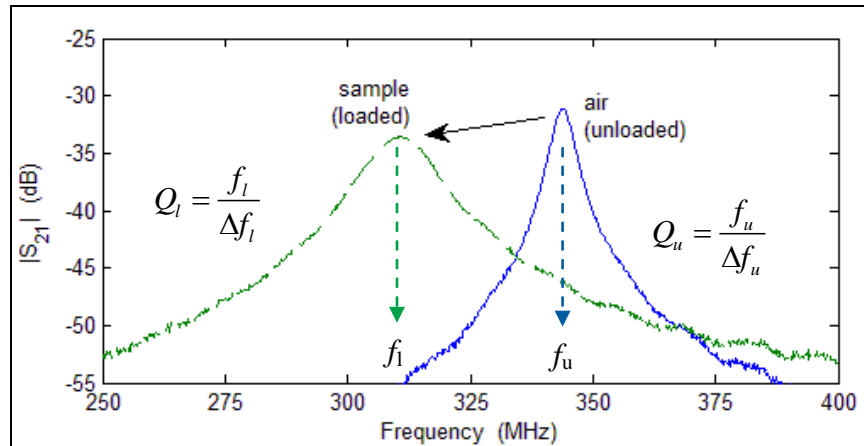


Figure 3. Data traces for permittivity measurement, before and after dielectric loading.

Each ring resonator has a characteristic $Re\{\epsilon_r\}$ -vs.-resonant-frequency curve. These curves are generated by repeated simulation using the procedure of the preceding paragraph and samples

with different dielectric constants. From the measured data, the ratio of the resonant peaks, f_1 / f_u , is calculated. This ratio maps to a particular value of $Re\{\epsilon_r\}$. A similar relationship is used to determine $Im\{\epsilon_r\}$ from Q_1 and Q_u . The equations necessary to compute $Re\{\epsilon_r\}$ and $Im\{\epsilon_r\}$ are found in references 2 and 8.

3. Measurement Equipment

The following equipment was used for the cold-soil study:

- 3 soil samples (approximately 75 in³ of each): 1 from Aberdeen Proving Ground, MD, 1 from Fort Irwin, CA, and 1 from Yuma Proving Ground, AZ
- 2 temperature-controlled chambers: Thermotron S-C8 (cold) and Yamato DKN400 (oven)
- 6 plastic cups (approximately 3 inches in diameter x 4 inches deep)
- 1 mass scale: Acculab VIC-5101
- 9 clear-plastic sample holders (approximately 5 in long x 5 in wide x 1 in deep)
- 1 roll of plastic-wrap
- 1 soil temperature monitor: Fluke 179 multimeter with thermocouple
- 1 cold chamber temperature monitor: Fisher Scientific 14-649-101 thermometer
- 2 ring resonators: 250 and 1200 MHz (Rogers 4350B PCBs)
- 1 aluminum weight: 4 in wide x 9 in long x 1.5 in deep, weighs 15.6 lb
- 2 coaxial cables, 15 ft long, with type Sub-Miniature Version A (SMA) connectors
- 1 network analyzer: Agilent N9923A “FieldFox”
- 1 keyboard with universal serial bus (USB) connector
- 1 personal computer (PC): Windows operating system, running Matlab

The soils are the samples under test. The temperature-controlled oven is used to bake the samples to 0% moisture initially. The temperature-controlled cold chamber is used to cool the samples from +30 °C down to -30 °C. The plastic cups and the scale are used to add 2% and 5% moisture to portions of the three soils. The clear-plastic containers hold each of the nine samples (3 soils x 3 moistures). The plastic wrap maintains the moisture of each sample and protects the ring resonators from contamination. The thermocouple attachment on the Fluke 179 multimeter is used to monitor the temperature of one of the soils inside the cold chamber. The Fisher

Scientific thermometer is used to monitor the temperature internal to the chamber after opening the door to make each measurement.

The two ring resonators are the dielectric measurement apparatus. The aluminum weight is placed on top of the ring resonator during the data capture to ensure flush contact between the sample and the ring. The coaxial cables connect the ring resonators to the network analyzer. The network analyzer records and stores $|S_{21}|$ data traces. The USB keyboard allows for convenient entry of an appropriate filename for each data trace. The PC is used—after all the data has been collected—to process the $|S_{21}|$ traces into ϵ_r .

The cold chamber, network analyzer, a ring resonator, the coaxial cables, and the USB keyboard are shown in figure 4a. The inside of the cold chamber, the soil samples, and the 250-MHz ring resonator are shown in figure 4b.

A close-up view of the data-capture pieces (network analyzer, ring resonator, cables, and keyboard) is shown in figure 5a. The Fluke 179 multimeter is shown in figure 5b.

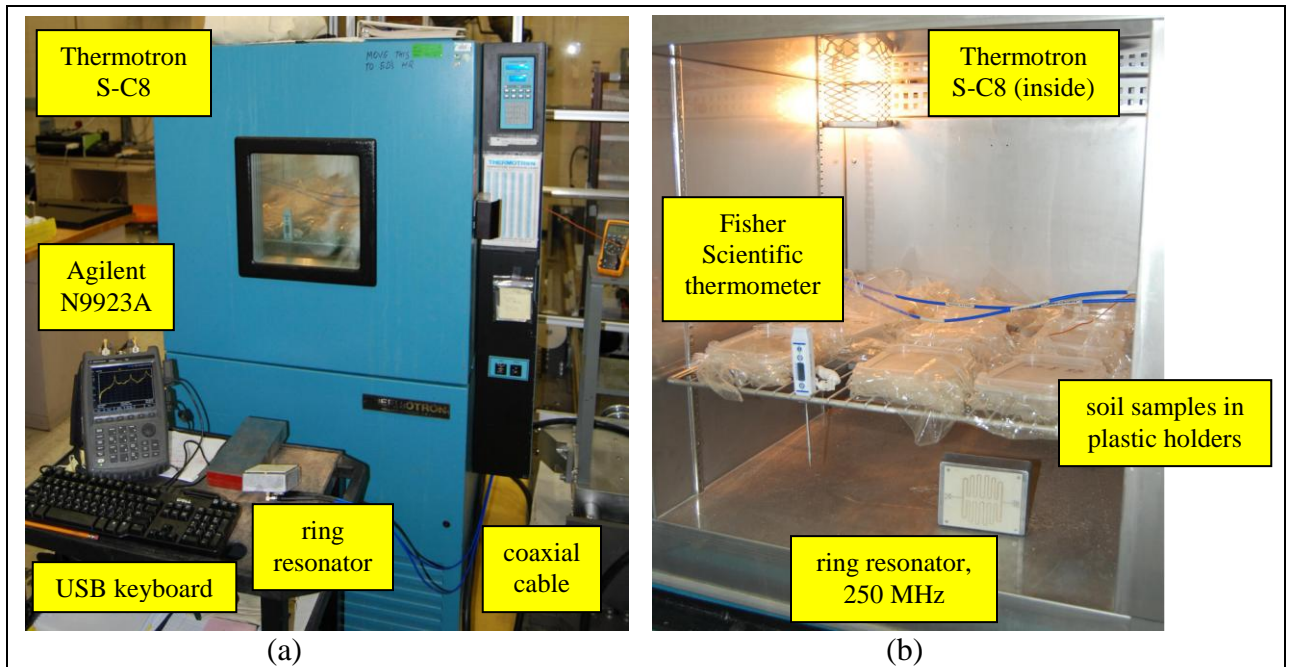


Figure 4. Thermotron S-C8 temperature-controlled chamber: (a) outside and (b) inside.

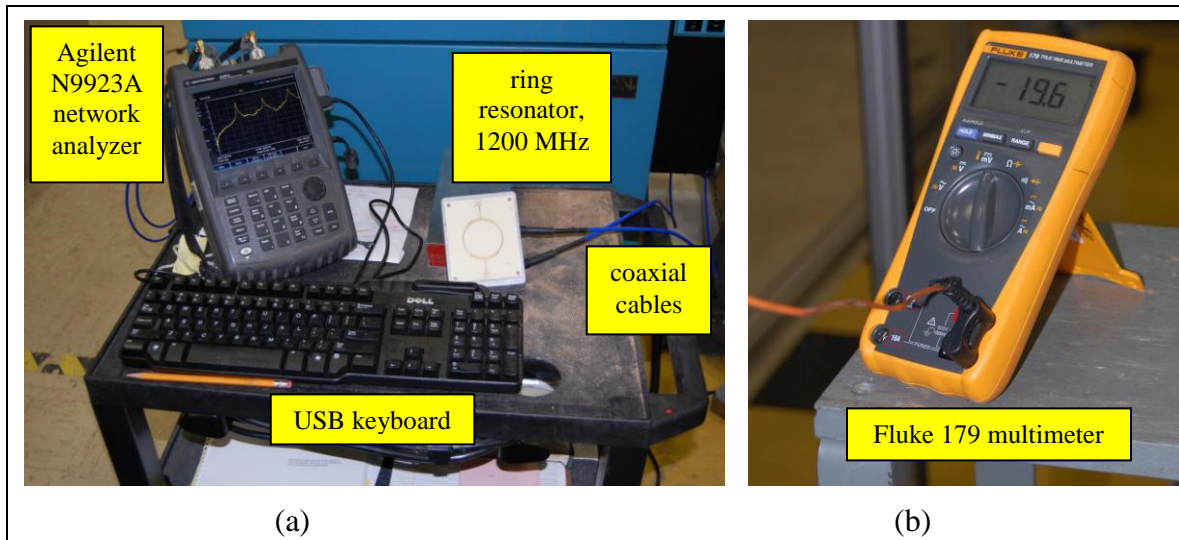


Figure 5. Measurement apparatus: (a) ring-resonator system and (b) temperature monitor.

4. Measurement Procedure

To prepare the soils for measurement, the following steps were taken:

1. Baked all three soils to 0% moisture using the Yamato DK400 oven,
2. Divided each soil into three equal parts and placed each division into its own cup (9 total),
3. Added distilled water to 1 cup of each soil to achieve 2% moisture-by-weight (3 total) and added distilled water to 1 cup of each soil to achieve 5% moisture-by-weight (3 total),
4. Lined nine plastic bins with plastic-wrap; emptied the contents of each cup into its own bin,
5. Placed the Fluke thermocouple inside one soil sample,
6. Covered each bin with a sheet of plastic wrap (to lock moisture in) and placed a lid on each plastic bin,
7. Placed the nine bins and two resonators into the Thermotron S-C8 cold chamber,
8. Routed the cable from the thermocouple to the outside of the chamber and routed the 15-ft coaxial cables from near one of the resonators to the outside of the cold chamber,
9. Set the temperature of the S-C8 to +30 °C and allowed the chamber to equilibrate,
10. Calibrated the Agilent N9923A for a two-port (S_{21}) measurement,
11. Plugged the USB keyboard into the N9923A, and
12. Waited 90 min for the temperature of the soils and resonators to equilibrate.

The rest of the measurement proceeded as shown in figure 6.

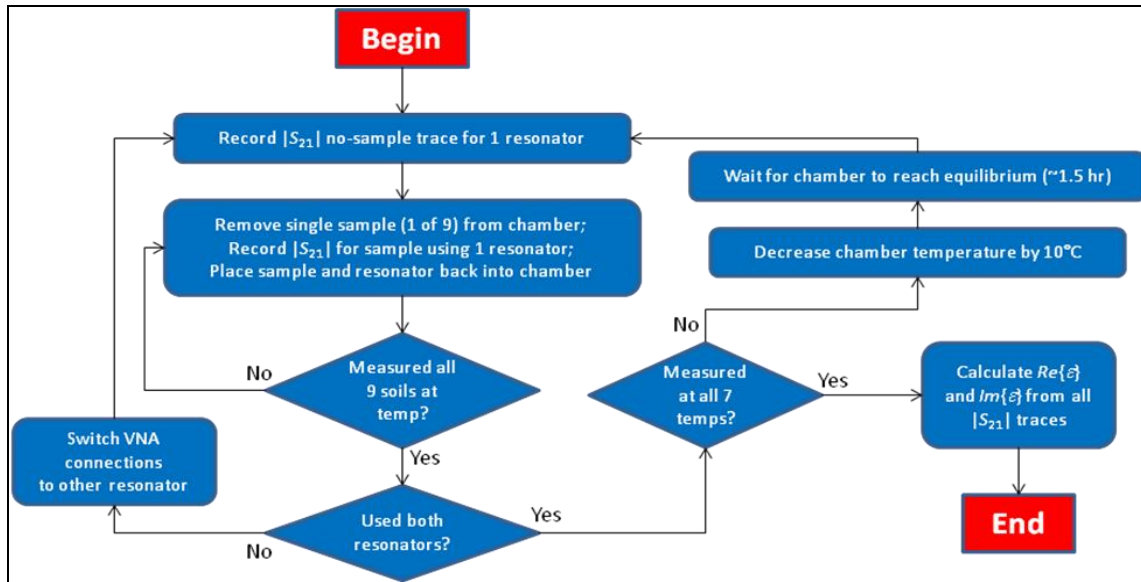


Figure 6. Measurement procedure flowchart.

At each temperature, $|S_{21}|$ for the no-sample case was recorded for the two resonators and then $|S_{21}|$ was measured for each soil sample, one at a time and with a short cool-down period in-between to maintain the cold temperature of all of the samples. The no-sample case is recorded with the resonator at the same temperature as the sample in order to minimize the effect of temperature on the measurement apparatus. (See the appendix for further information.)

One of the sample-present data captures is shown in figure 7. In figure 7a, the plastic-wrap holding the sample is opened momentarily, and the resonator is inverted and placed flush against the soil. In figure 7b, the aluminum weight is placed above the resonator to press it against the sample and the $|S_{21}|$ trace is recorded on the network analyzer.

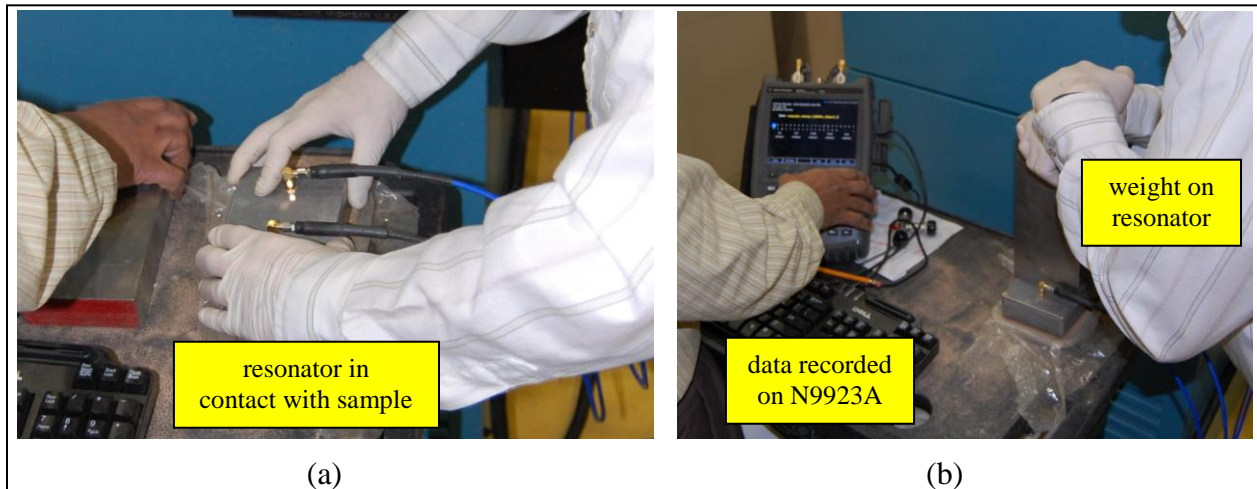


Figure 7. Data capture example: (a) place the ring resonator in flush contact with the sample and (b) record the associated $|S_{21}|$ trace on the VNA.

To cool the soils down to the next temperature, the chamber was left sealed for 90 min; afterwards, the no-sample and sample data traces were recorded as before. The entire procedure was repeated at every 10°, from +30 °C down to -30 °C. Thus, $|S_{21}|$ data were recorded for three different soil types, at three different percent-moisture contents, and at seven different temperatures for two resonators.

After all the traces were collected, the data were downloaded from the network analyzer to the PC and the “N9923A_ringres” Matlab script was executed. A screenshot of the graphical user interface (GUI) is given in figure 8. From this GUI, the user loads the no-sample and sample traces and directs Matlab to calculate $Re\{\epsilon_r\}$ and $Im\{\epsilon_r\}$ from the equations programmed into the script. For all samples, the dielectric constant was processed for the 250-MHz resonator at four harmonics (250, 500, 750, and 1000 MHz) and for the 1200-MHz resonator at three harmonics (1200, 2400, and 3600 MHz).

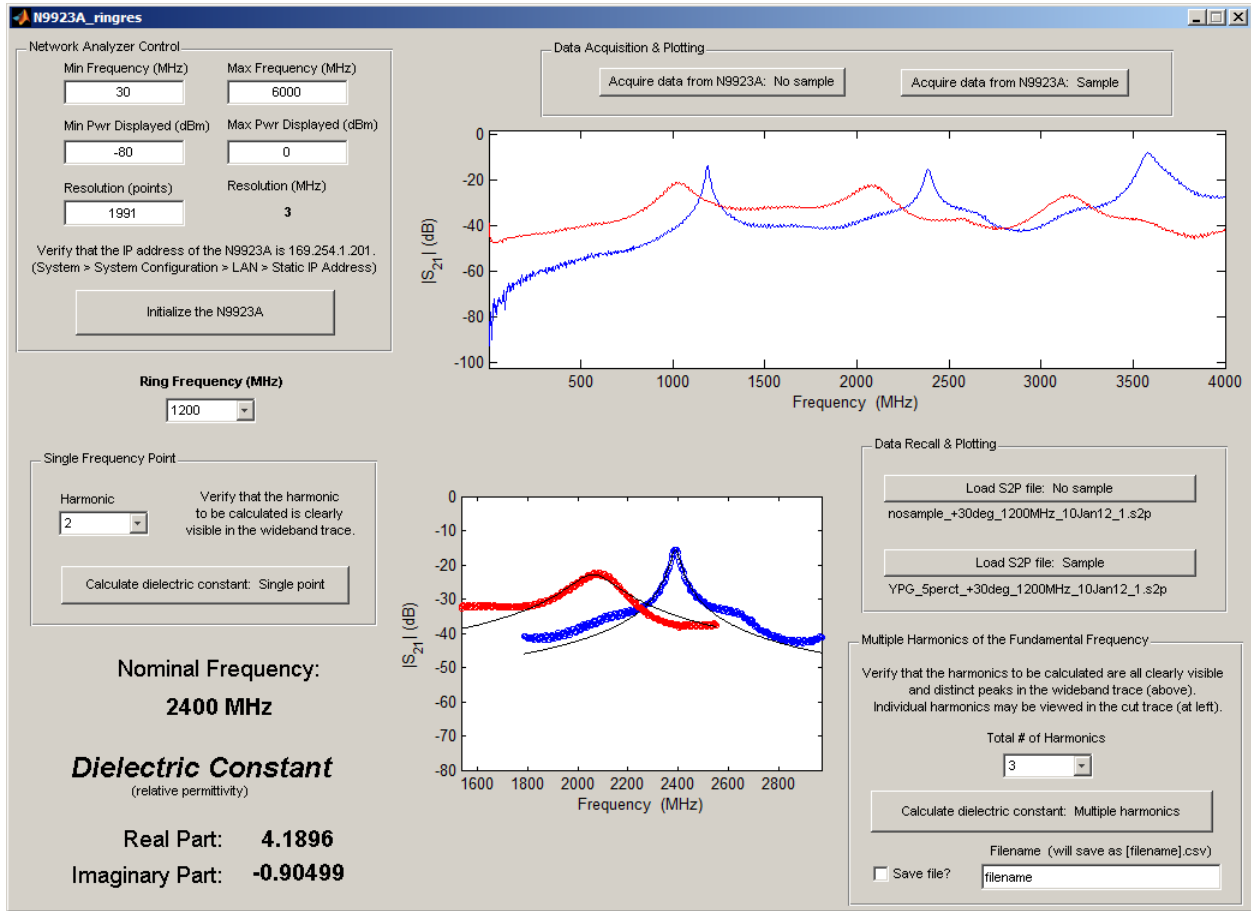


Figure 8. N9923A_ringres GUI: the sample-absent trace is shown in blue; the sample-present trace is shown in red.

5. Dielectric Constant Data

The data collected during this study are given in figures 9 through 20. For figures 9 through 14, the magnitudes of $Re\{\epsilon_r\}$ and $Im\{\epsilon_r\}$ are shown in grayscale. The data have been interpolated between the seven temperatures and 3%-moisture data points to provide smooth shading transitions in all plots. For figures 15 through 20, $Re\{\epsilon_r\}$ and $Im\{\epsilon_r\}$ are plotted against temperature for three sample frequencies. Within each plot are the traces corresponding to the three moisture levels.

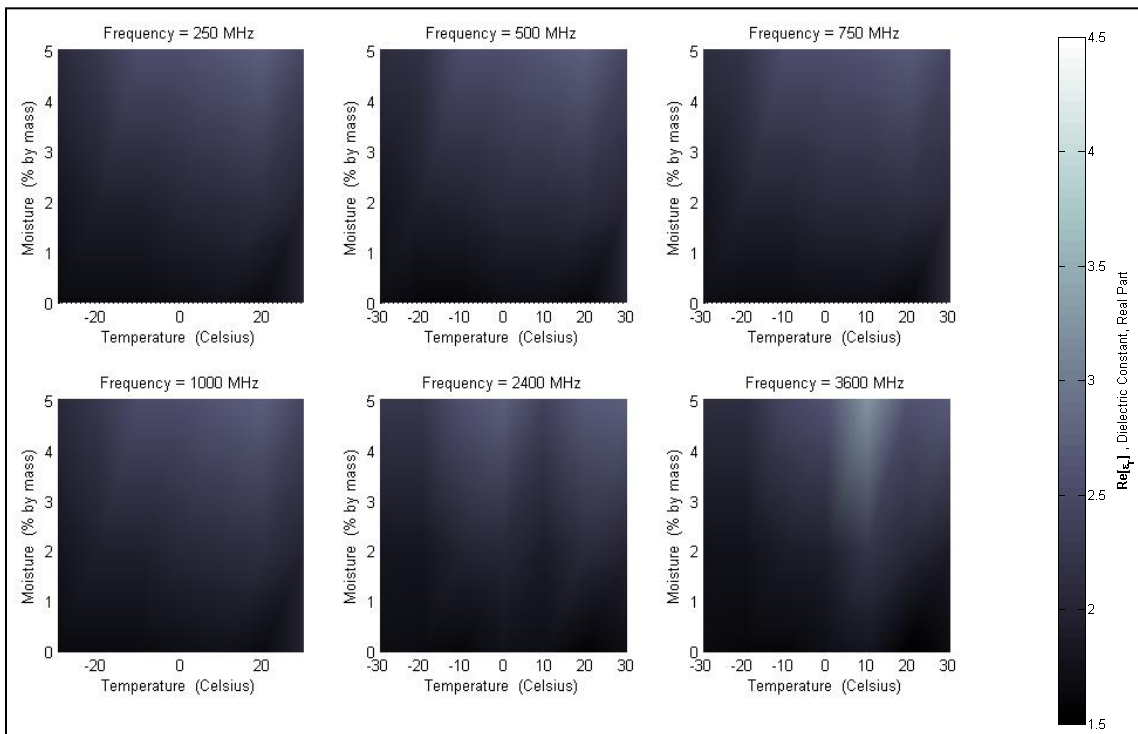


Figure 9. Dielectric constant (real part) vs. temperature and moisture, APG soil.

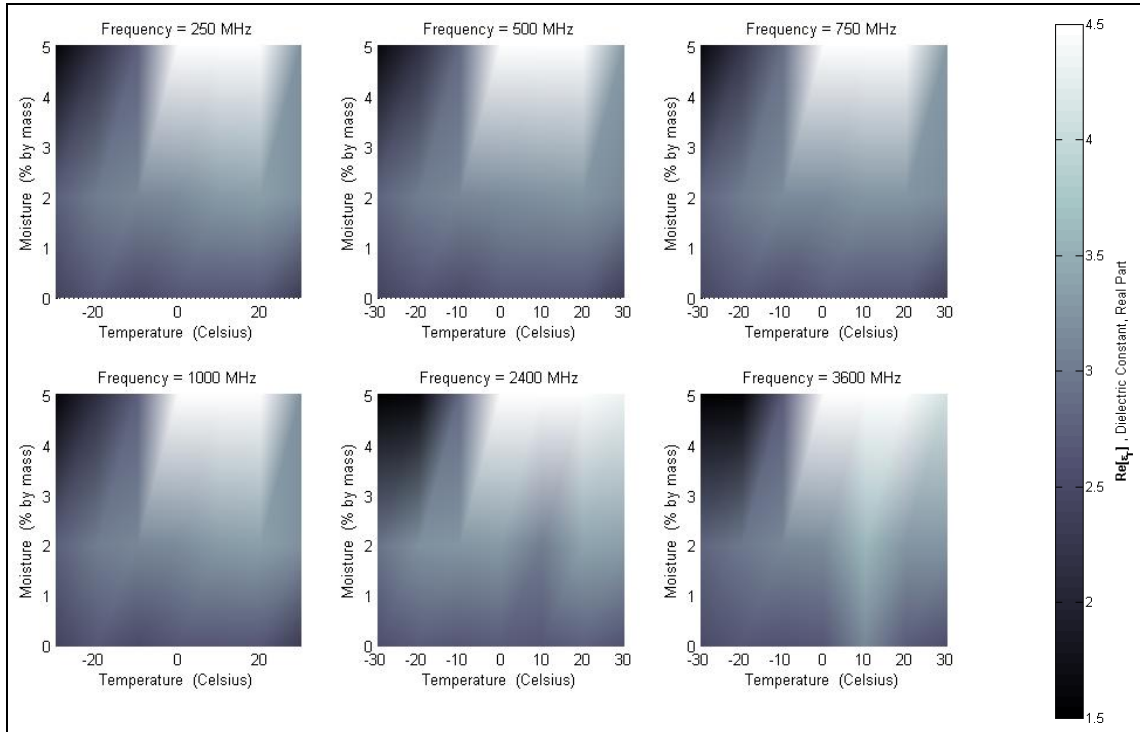


Figure 10. Dielectric constant (real part) vs. temperature and moisture, Ft. Irwin soil.

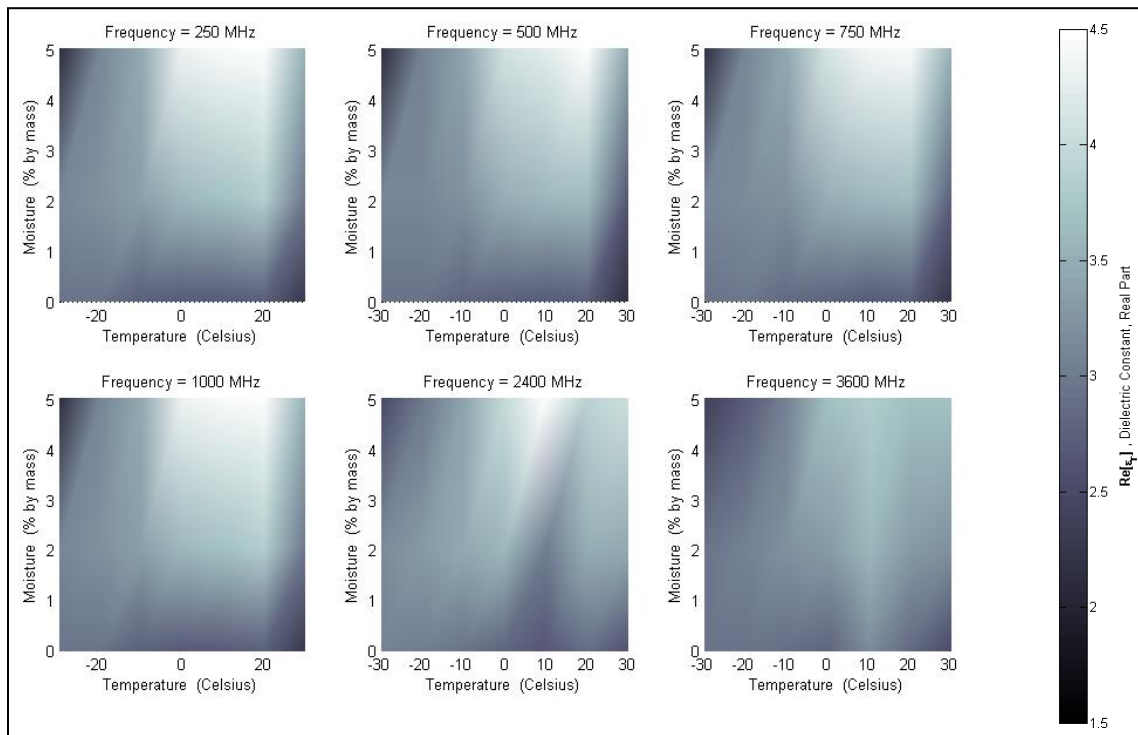


Figure 11. Dielectric constant (real part) vs. temperature and moisture, YPG soil.

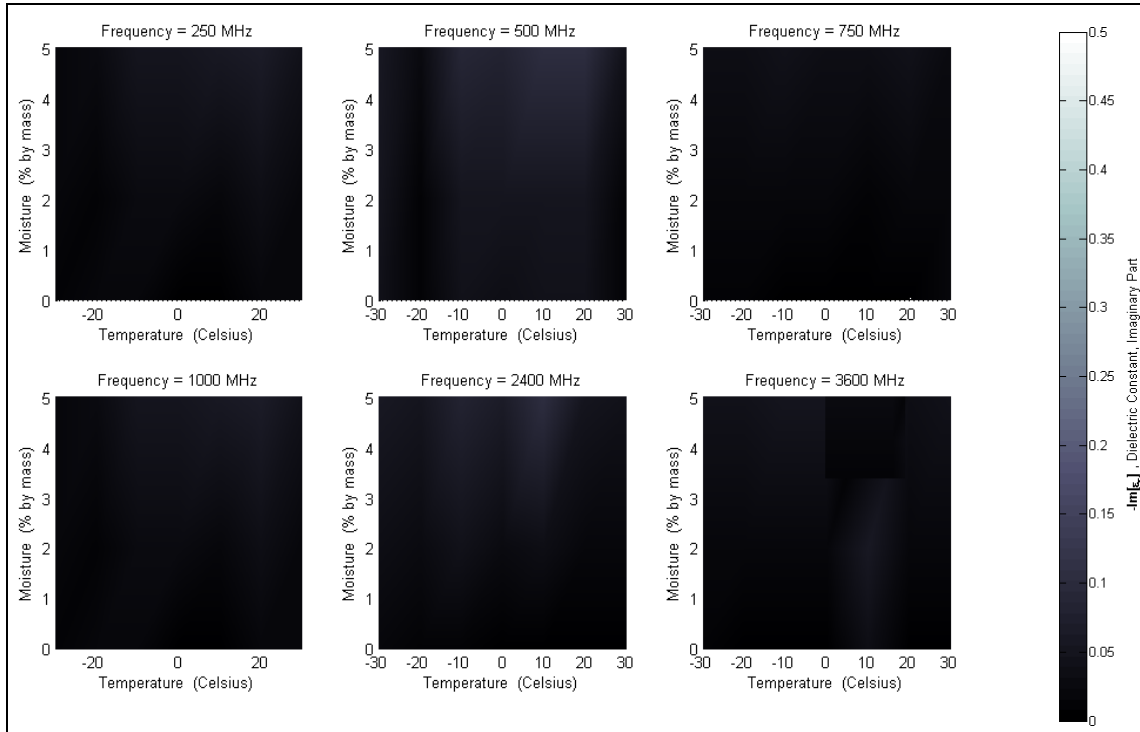


Figure 12. Dielectric constant (imaginary part) vs. temperature and moisture, APG soil.

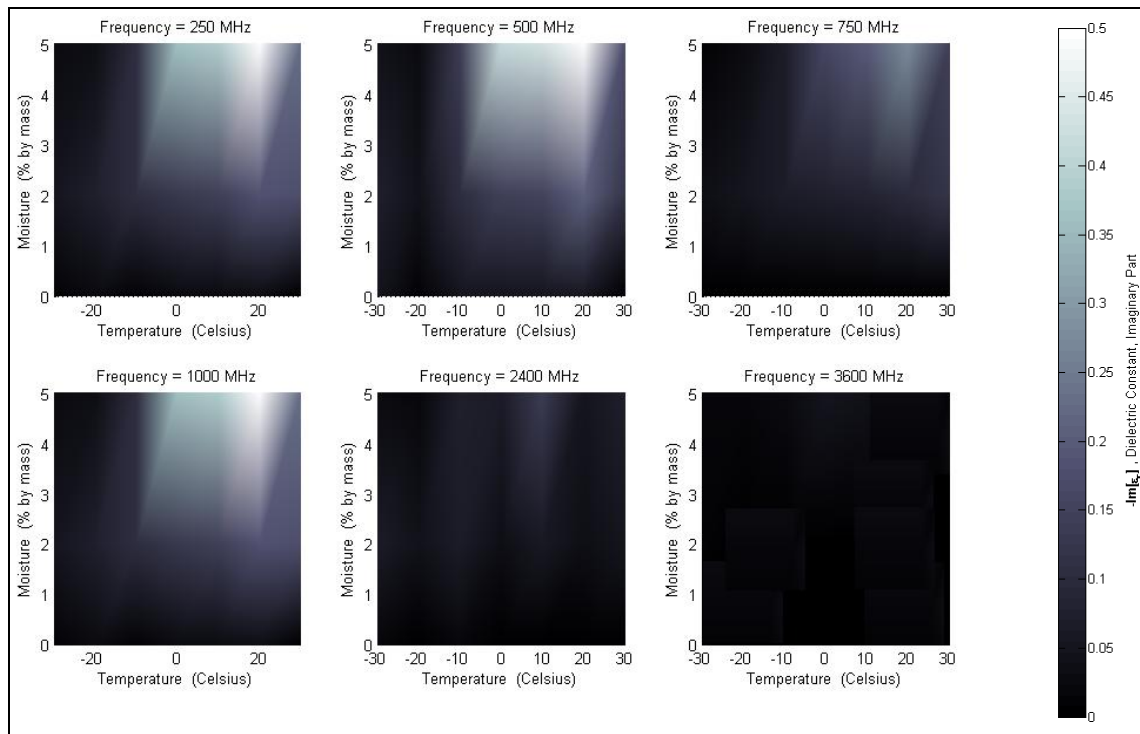


Figure 13. Dielectric constant (imaginary part) vs. temperature and moisture, Ft. Irwin soil.

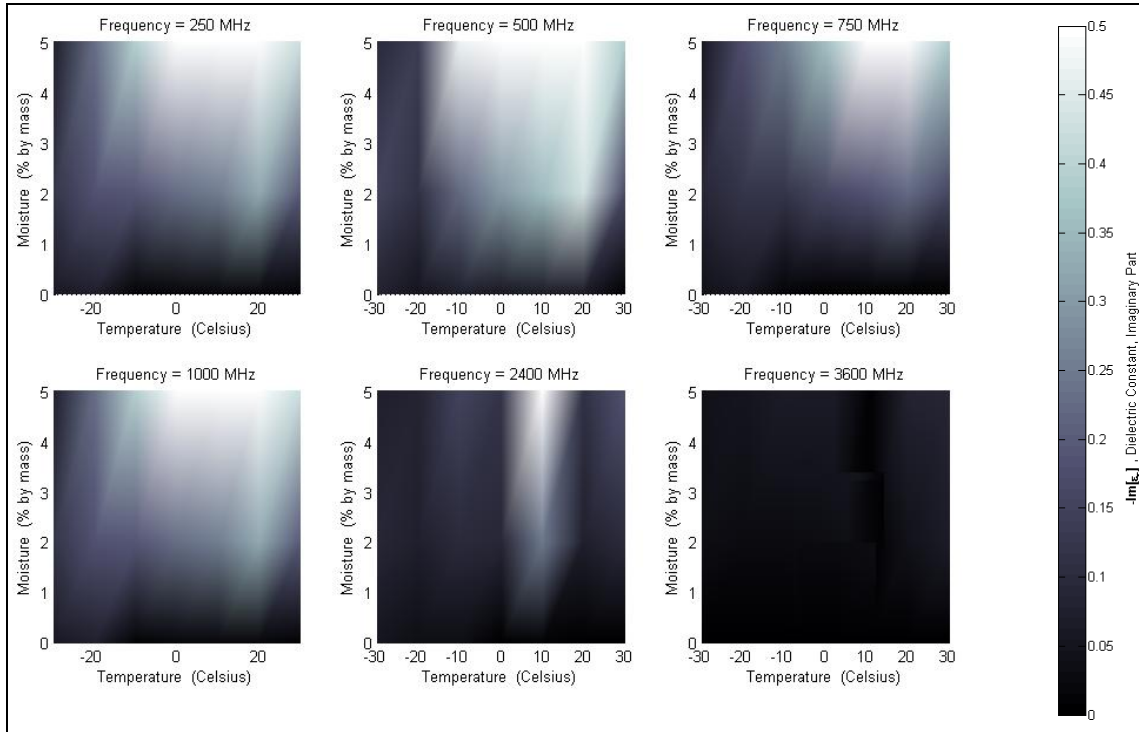


Figure 14. Dielectric constant (imaginary part) vs. temperature and moisture, YPG soil.

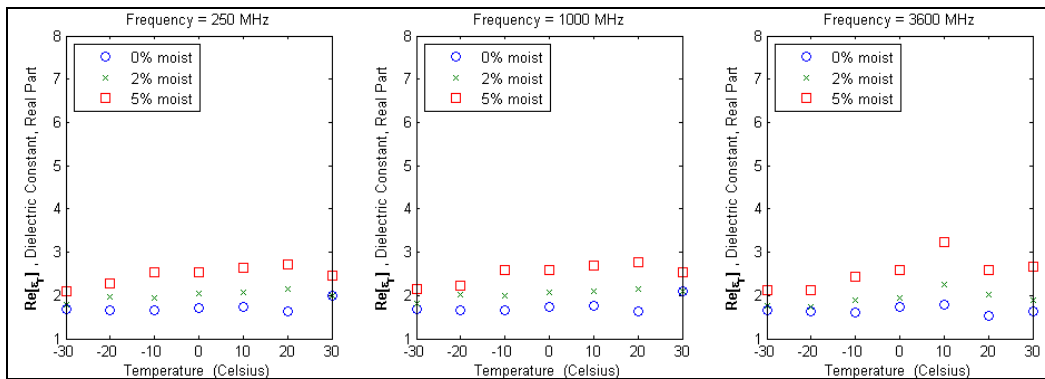


Figure 15. Dielectric constant (real part) vs. temperature, APG soil.

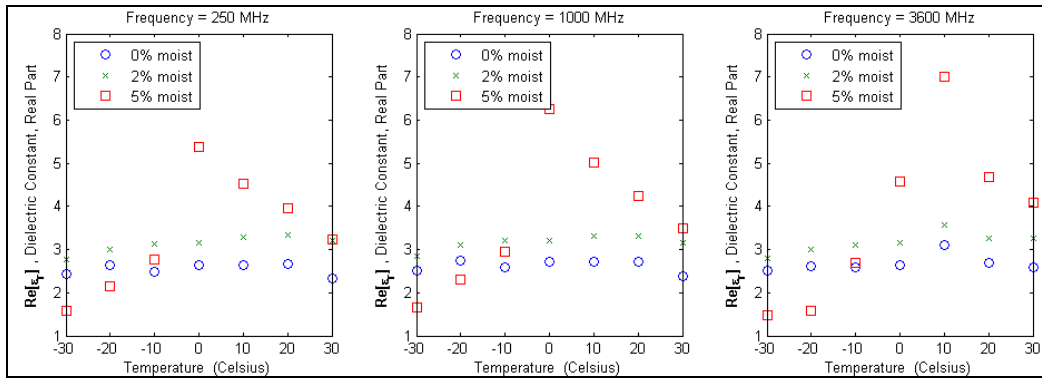


Figure 16. Dielectric constant (real part) vs. temperature, Ft. Irwin soil.

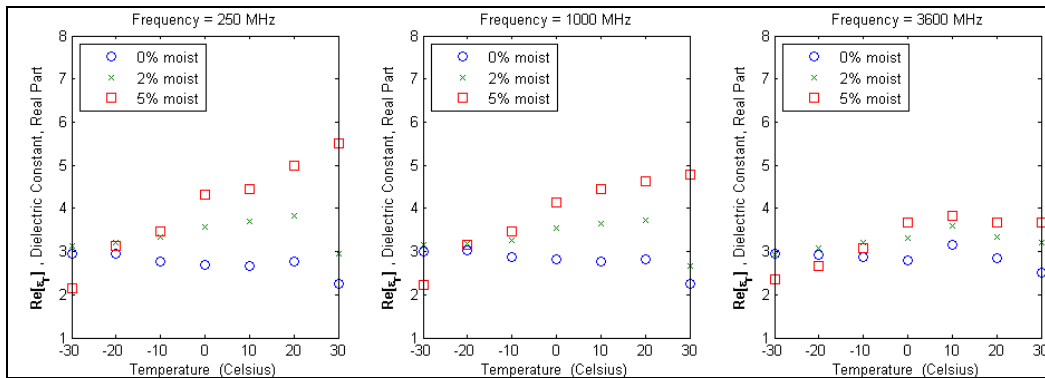


Figure 17. Dielectric constant (real part) vs. temperature, YPG soil.

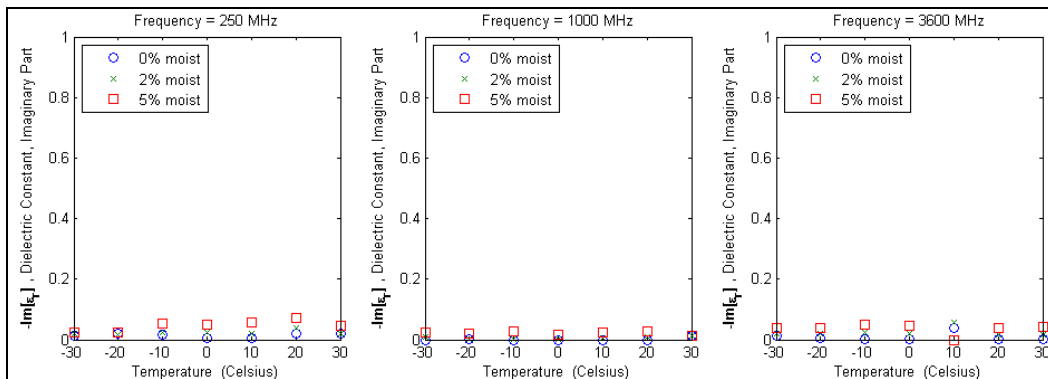


Figure 18. Dielectric constant (imaginary part) vs. temperature, APG soil.

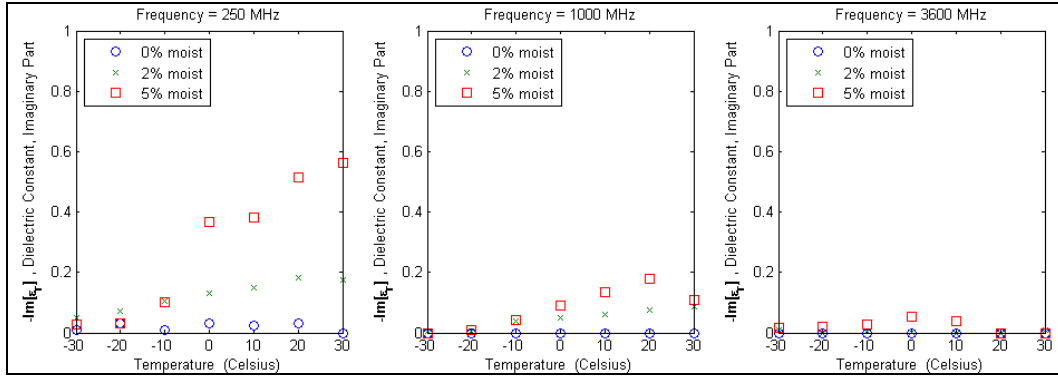


Figure 19. Dielectric constant (imaginary part) vs. temperature, Ft. Irwin soil.

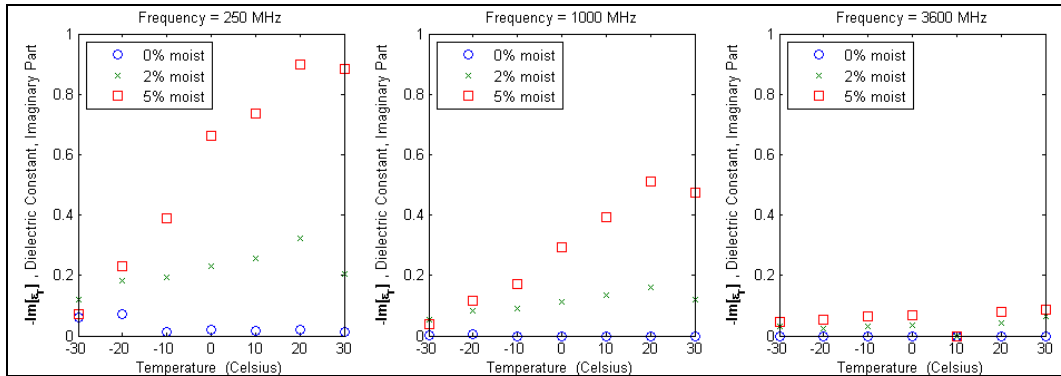


Figure 20. Dielectric constant (imaginary part) vs. temperature, YPG soil.

The following trends are observed in the grayscale plots (figures 9–14):

- For the APG soil, little variation in $Re\{\epsilon_r\}$ and $Im\{\epsilon_r\}$ is observed across moisture and temperature variations.
- For the Ft. Irwin soil and 0% or 2% moisture, there is little variation in $Re\{\epsilon_r\}$ and $Im\{\epsilon_r\}$.
- For the Ft. Irwin soil and 5% moisture, there is considerable variation in $Re\{\epsilon_r\}$ and $Im\{\epsilon_r\}$ across temperature: both $Re\{\epsilon_r\}$ and $Im\{\epsilon_r\}$ drop when the sample is cooled.
- For the YPG soil, the drop in $Re\{\epsilon_r\}$ and $Im\{\epsilon_r\}$ is not as distinct but still evident.

The following trends are observed in the overlaid traces (figures 15–20):

- The APG soil shows a constant $Re\{\epsilon_r\}$ for 0%, 2%, and 5% moisture versus temperature.
- The Ft. Irwin soil shows a constant $Re\{\epsilon_r\}$ for 0% and 2% moisture, and a step-like change in $Re\{\epsilon_r\}$ for 5% moisture near 0 °C.
- The YPG soil shows a constant $Re\{\epsilon_r\}$ for 0% moisture, a slight linear rise in $Re\{\epsilon_r\}$ with temperature for 2% moisture, and a more distinct, nearly linear rise in $Re\{\epsilon_r\}$ with temperature for 5% moisture.

- The APG soil shows a constant $Im\{\varepsilon_r\}$ near zero for all three moisture levels.
- The Ft. Irwin soil shows a near-zero $Im\{\varepsilon_r\}$ for 0% moisture, a linear rise in $Im\{\varepsilon_r\}$ for 2% moisture, and a sharper rise in $Im\{\varepsilon_r\}$ for 5% moisture (for two of three frequencies).
- The YPG soil shows a near-zero $Im\{\varepsilon_r\}$ for 0% moisture, a linear rise in $Im\{\varepsilon_r\}$ for 2% moisture, and a sharper linear rise in $Im\{\varepsilon_r\}$ across temperature for 5% moisture (for two of three frequencies).
- For constant temperature, constant moisture, and increasing frequency, $Re\{\varepsilon_r\}$ remains nearly constant while $Im\{\varepsilon_r\}$ drops sharply.

Our results generally confirm those presented previously (3, 4). New information generated by this study relevant to GPR performance is as follows:

- There is little variation in ε_r across temperature for dry soils. With regards to EM wave interactions with dielectrics in the environment, it is expected that radar performance will neither be degraded nor improved.
- For moderate soil moisture content (e.g., 2%-by-weight), there will be a mild drop in both $Re\{\varepsilon_r\}$ and $Im\{\varepsilon_r\}$. From +30 °C down to -30 °C, the drop in $Re\{\varepsilon_r\}$ is expected to be less than 10%. Assuming that $Re\{\varepsilon_r\}$ for the target and soil are approximately equal at/near room temperature, the contrast between target and soil is improved at the cold temperature but only minimally. From +30 °C down to -30 °C, the drop in $Im\{\varepsilon_r\}$ can be as high as 70%; thus, radar penetration into the soil may improve considerably.
- For high soil moisture content (e.g., 5%-by-weight), there can be a significant drop (step-change) in both $Re\{\varepsilon_r\}$ and $Im\{\varepsilon_r\}$ below the freezing point of water. $Re\{\varepsilon_r\}$ can drop by as much as 50% and $Im\{\varepsilon_r\}$ can drop by as much as 90%. It is expected that both the contrast between the soil and target as well as the penetration depth into the soil will increase.
- The step-change in ε_r for high moisture contents is believed to be due to the phase change of the moisture from liquid to solid. Above the freezing point, the soil's water/particulate mixture is (1) highly polarizable, thus $Re\{\varepsilon_r\}$ is high, and (2) lossy, thus $Im\{\varepsilon_r\}$ is also high. Below the moisture freezing point, the soil is not very polarizable, thus ε_r approaches that of air, i.e., the value of $Re\{\varepsilon_r\}$ approaches 1 and the value of $Im\{\varepsilon_r\}$ approaches 0.

6. Conclusion

Our results have shown that (1) for dry soil, cold temperatures have little effect on the dielectric constant and (2) for soils with medium and high moisture contents, there is a downward trend in $Re\{\varepsilon_r\}$ and $Im\{\varepsilon_r\}$ for cold temperatures. A step-change in ε_r is observed for soil with high moisture contents just below 0 °C, apparently due to the phase change of the moisture from liquid to solid.

With respect to variations in ε_r , for dry soils, the performance of counter-improvised explosive device (IED) radar sensors is expected to remain steady at cold temperatures. For medium and high moisture content soils, an increase in radar penetration into the soil is expected for cold temperatures. Also, for medium and high moisture content soils, assuming that $Re\{\varepsilon_r\}$ for the target and soil are approximately equal at/near room temperature, an increase in soil-to-target contrast is expected.

7. References

1. Smith, G. D. *U.S. Army Research Laboratory (ARL) Very High Frequency (VHF)/Ultra High Frequency (UHF) Permittivity Measurement Software: Data Capture and Reduction*; ARL-TR-4780; U.S. Army Research Laboratory: Adelphi, MD, April 2009.
2. Mazzaro, G.; Sherbondy, K.; Smith, G.; Ressler, M.; Harris, R. *Portable Ring-resonator Permittivity Measurement System: Design & Operation*; unpublished; U.S. Army Research Laboratory: Adelphi, MD, December 2011.
3. Zhang, L.; Shi, J.; Zhang, Z.; Zhao, K. The Estimation of Dielectric Constant of Frozen Soil-water Mixture at Microwave Bands. *IEEE International Geoscience and Remote Sensing Symposium* **July 2003**, 4, 2903–2905.
4. Mironov, V. L.; De Roo, R. D.; Savin, I. V. Temperature-dependable Microwave Dielectric Model for an Arctic Soil. *IEEE Transactions on Geoscience and Remote Sensing* **June 2010**, 48 (6), 2544–2556.
5. Jaganathan, A. P.; Allouche, E. Z. Temperature Dependence of Dielectric Properties of Moist Soils. *Canadian Geotechnical Journal* **June 2008**, 45 (6), 888–894.
6. Chang, K.; Hsieh, L. H. *Analysis and Modeling of Ring Resonators*; in *Microwave Ring Circuits and Related Structures*, 2nd ed., Hoboken, NJ: John Wiley & Sons, 2004, h. 2, Sec. 2.2, pp. 6–7.
7. Sarabandi, K.; Li, E. S. Microstrip Ring Resonator for Soil Moisture Measurements. *IEEE Transactions on Geoscience and Remote Sensing* **Sept. 1997**, 35 (5), 1223–1231.
8. Mazzaro, G.; Sherbondy, K.; Smith, G.; Hu, J. Portable Ring Resonator Permittivity Measurement System. *57th Annual Meeting of the MSS Tri-Service Radar Symposium*, Monterey, CA, June 2011.

Appendix. Effect of Cold Temperature on the Ring-Resonator Measurement System

Data traces were recorded from the two resonators (with no sample present) at room temperature and each cold temperature in order to observe the effect of temperature on the measurement apparatus.

Figure A-1 provides a sample pair of traces for the 2nd harmonic of the 1200-MHz resonator. The trace recorded at room temperature is in dashed-black; the trace recorded at $-30\text{ }^{\circ}\text{C}$ is in solid-blue. For the cold temperature, compared to room temperature, (1) the frequency of the resonance shifts slightly upward and (2) the quality factor of the resonance remains approximately the same.

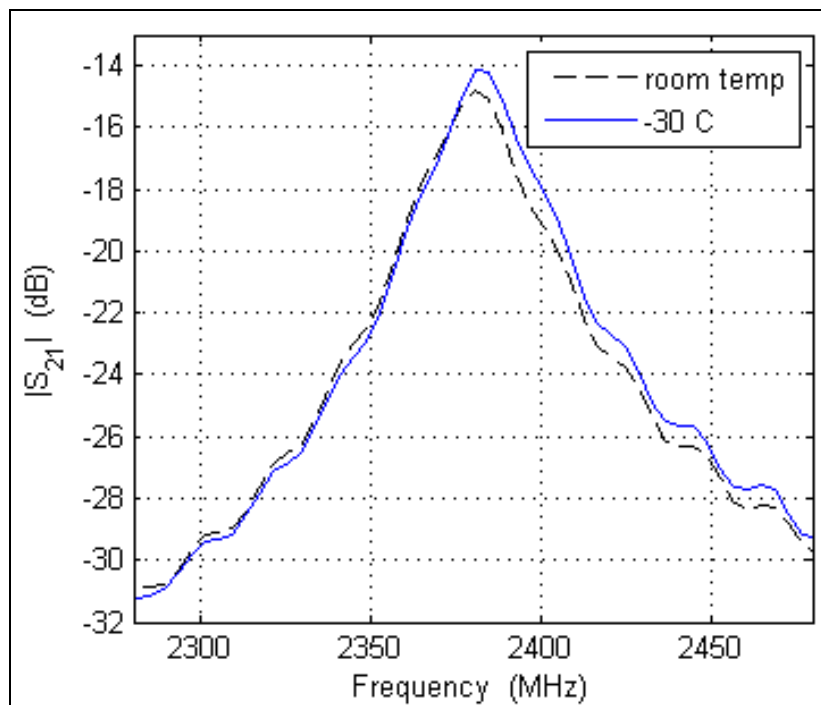


Figure A-1. Dielectric constant (imaginary part) vs. temperature, YPG soil.

For all temperatures, resonators, and harmonics considered in this study, the shift in resonance was observed to be less than 2% and the quality-factor change in the peak was observed to be less than 1%. While these changes are minimal, they can affect the values for ϵ_r calculated for each sample. To counteract this temperature effect on the measurement apparatus, the no-sample traces were recorded at the same temperature as each sample. For each percent-moisture, temperature, and frequency, the calculation of ϵ_r was performed by comparing the resonant shift and quality factor change from the sample-absent case to the sample-present case at the same temperature.

NO. OF
COPIES ORGANIZATION

- 1 (PDF only) DEFENSE TECHNICAL INFORMATION CTR
DTIC OCA
8725 JOHN J KINGMAN RD
STE 0944
FORT BELVOIR VA 22060-6218
- 1 DIRECTOR
US ARMY RESEARCH LAB
IMNE ALC HRR
2800 POWDER MILL RD
ADELPHI MD 20783-1197
- 1 DIRECTOR
US ARMY RESEARCH LAB
RDRL CIO LL
2800 POWDER MILL RD
ADELPHI MD 20783-1197
- 1 DIRECTOR
US ARMY RESEARCH LAB
RDRL CIO LT
2800 POWDER MILL RD
ADELPHI MD 20783-1197
- 2 NIGHT VISION & ELECTRONIC SENSORS DIRECTORATE
ATTN RDER-NVS-IT MARC TITLER
ATTN AMSRD CER NV CM GVA B BARLOW
10221 BURBECK RD
FT BELVOIR VA 22060-5806
- 10 DIRECTOR
US ARMY RESEARCH LAB
ATTN RDRL-SER-U
ROBERTO INNOCENTI
KARL KAPPRA
GETACHEW KIROSE
GREGORY MAZZARO
LAM NGUYEN
KENNETH RANNEY
MARC RESSLER
KELLY SHERBONDY
GREGORY SMITH
ANDERS SULLIVAN
2800 POWDER MILL RD
ADELPHI MD 20783-1197

TOTAL: 16 (1 ELEC, 15 HCS)